Editors' Suggestion

Nonthermal current-induced transition from skyrmion lattice to nontopological magnetic phase in spatially confined MnSi

Takuro Sato,[1,*] Wataru Koshibae,[1] Akiko Kikkawa,[1] Yasujiro Taguchi,[1] Naoto Nagaosa,[1,2] Yoshinori Tokura,[1,2,3] and Fumitaka Kagawa[1,2,†]

[1]*RIKEN Center for Emergent Matter Science (CEMS), Wako 351-0198, Japan*
[2]*Department of Applied Physics, University of Tokyo, Tokyo 113-8656, Japan*
[3]*Tokyo College, University of Tokyo, Tokyo 113-8656, Japan*

(Received 24 February 2022; revised 7 September 2022; accepted 23 September 2022; published 21 October 2022)

An electronic/magnetic order often turns into a different phase of matter when the temperature, pressure, or magnetic field varies, and resulting changes in physical quantities form the basis of various switching devices. By contrast, global phase changes triggered by electric current with minimal Joule heating often remain elusive, although it may offer exotic possibilities for phase manipulation in micro/nanoscale materials. Here, we report the experimental and numerical realizations of a nonthermal current-induced magnetic transition for a spatially confined skyrmion-hosting system. In a microfabricated MnSi, the application of a DC current triggers a nonvolatile suppression of the topological Hall effect, comparable in magnitude to that observed for the skyrmion-to-nonskyrmion thermodynamic transition of the whole system. A similar current-induced global transition is also found in numerical simulations with open boundaries. These phenomena are not seen either in the corresponding bulk system or in the simulation with periodic boundaries, thus, indicating a key role of the confined geometry in the nonthermodynamic phase change triggered by current.

DOI: 10.1103/PhysRevB.106.144425

I. INTRODUCTION

Global phase control by external stimuli is one of the promising directions for designing giant responses in solid-state devices. Equilibrium thermodynamics, or thermodynamic free energy, provides a firm basis for phase control by environmental parameters, such as temperature, pressure, or magnetic field. Phase control by electric current, if feasible, may be an even more tantalizing direction when considering the implementation of such phase-control devices in modern or next-generation nanoscale electronics. From an academic point of view, however, a material with current flowing is in a nonequilibrium state, and the general understanding of phase control by nonthermodynamic pathways, such as current, is quite challenging. The experimental realization of current-induced phase changes, which may be called nonequilibrium phase transition if it is not driven merely by a thermal effect (Joule heating), have been extensively studied, for instance, in insulator-to-metal transitions in correlated electron systems [1–9].

Recently, versatile current-induced spin dynamics in itinerant magnets have been demonstrated experimentally, such as ferromagnetic domain-wall motion [10–12], magnetization reversal [13–15], and precession of magnetization [16–18]. Theoretically, these nonlinear behaviors are well described in terms of spin currents and their interactions with magnetism [19], and at present, numerical simulations have become a powerful method for studying nonequilibrium spin dynamics under electric currents. Furthermore, some numerical studies point to possibilities for current-induced phase transitions in magnetic symmetry, for instance, from antiferromagnetic to ferromagnetic phases in a heterostructured system [20]. These recent advances indicate that spin systems in itinerant magnets may provide another platform to explore phase transitions driven by current.

In the present paper, we pursue the experimental realization of current-induced global phase changes in magnetism by targeting skyrmions, nanometer-sized magnetic vortices characterized by integer topological numbers [21–25]. Previous studies have established that magnetic skyrmions can exhibit translational motion under a DC electric current [26–30], and a steady skyrmion flow is indeed realized in bulk [31,32] or periodic-boundary systems [29,33,34]. Whereas such skyrmion translational motion is not accompanied by a change in the macroscopic magnetic symmetry, such as a neutron-diffraction pattern [31], magnetic phase changes from helimagnetic/ferromagnetic to skyrmionic states are also found numerically in periodic-boundary systems at a current density much higher than that required for the translational motion [29,35]. However, nonequilibrium states under a steady current may further be different in small-sized or open-boundary systems. To sustain a steady skyrmion flow, the skyrmion creation rate on one boundary of the sample, and the skyrmion annihilation rate on the opposite boundary must be balanced, whereas a continuous change in the magnetic texture is not allowed for topological reasons. This seemingly incompatible situation would be a stringent constraint in a system with a large surface-to-volume ratio, leading us to

*takurosato@ims.ac.jp
†kagawa@phys.titech.ac.jp

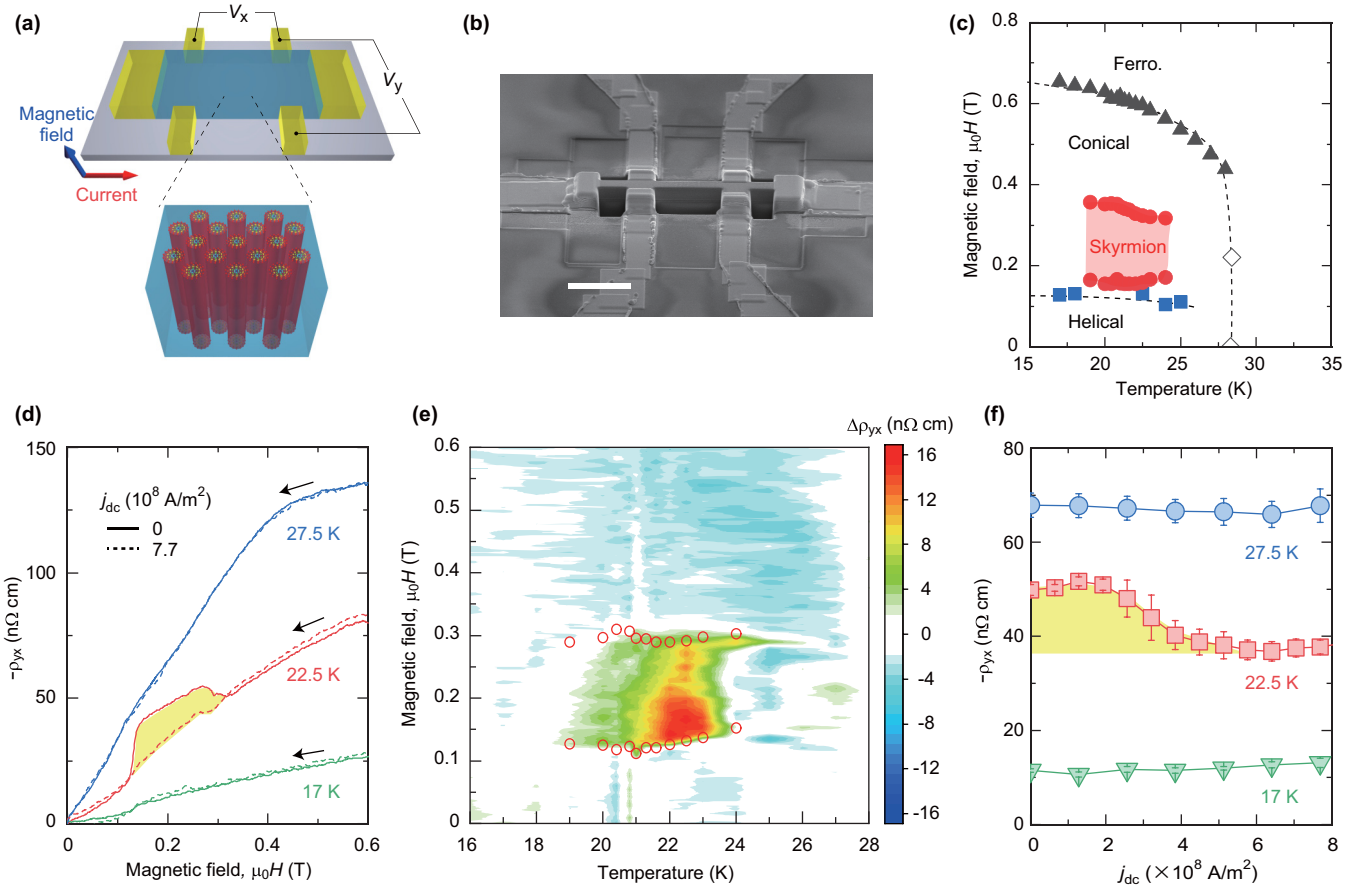

FIG. 1. Suppression of the topological Hall effect under a DC electric current in microfabricated MnSi. (a) Schematic of the experimental configuration. An external magnetic field was applied along the [001] axis, perpendicular to the CaF_2 substrate. An electric current was applied along the long axis of the device. The longitudinal and Hall voltages (V_x and V_y, respectively) were measured at the two different sets of electrodes. (b) Scanning electron microscope image of the microfabricated MnSi used in this paper. The scale bar represents 5 μm. (c) Equilibrium magnetic phase diagram of the present specimen. The skyrmion phase boundaries were determined from the ρ_{yx}–H profiles as the midpoint of the hysteresis that was observed during the field-increasing and field-decreasing processes. (d) Hall resistivity as a function of magnetic field with/without a DC electric current bias (7.7×10^8 A/m^2) at selected temperatures. The topological Hall effect (THE), which signifies the skyrmion phase, is highlighted by yellow shading. The data were recorded during the field-decreasing process. The magnitude of the THE is consistent with that observed in bulk MnSi at a similar temperature [42]. (e) Color plot of the current-induced change in the Hall resistivity. Red open circles delimit the region in which the THE is appreciable during the field-decreasing process under no DC current. (f) Typical variations in the Hall resistivity as a function of the DC current bias at $\mu_0 H = 0.22$ T. The yellow shaded region represents the contribution of the THE shown in (d). The measurements were performed at $\mu_0 H = 0.22$ T.

envisage that another form of a nonequilibrium state, such as a global phase transition that has not been found either experimentally or numerically, may emerge in such a spatially confined system.

II. RESULTS AND DISCUSSION

A. Sample preparations

Given this working hypothesis, we first performed experiments on a microfabricated system. A MnSi bulk crystal, a chiral magnet exhibiting a skyrmion lattice phase with a skyrmion spacing of ∼20 nm [23,36,37] was fabricated with micrometer dimensions ($18.0\times1.3\times1.2$ μm^3) using a focused ion beam (FIB) and transferred onto a CaF_2 substrate [Figs. 1(a) and 1(b)]. We found that the overall transport characteristics, such as the longitudinal, ordinary Hall, and anomalous Hall resistivities including their sign (Fig. S1 in the Supplemental Material [38]), are qualitatively similar to those in a bulk MnSi specimen [39], and we, thus, constructed the thermodynamic phase diagram of the present specimen as shown in Fig. 1(c). Figure 1(d) displays the Hall resistivity ρ_{yx} at selected temperatures T as a function of the magnetic-field H. The Hall resistivity was measured with a lock-in technique (see Materials and Methods), and the presence of the skyrmion phase was confirmed from the emergence of a top-hat-shaped increase in the Hall voltage [the THE [36,40,41]; see the solid curve measured at 22.5 K in Fig. 1(d)]. The magnitude of the THE is 13 to 14 nΩ cm at 22.5 K, which is nearly the same with the value of the (quenched) skyrmion phase in bulk MnSi at the same temperature [42]. In the obtained phase diagram, the skyrmion phase is observed in 19–24 K, which is appreciably lower than the case of the bulk phase diagram 27–29 K [23]. This difference is attributable to the fact that the microfabricated MnSi is fixed to the CaF_2 substrate and,

thus, at low temperatures the present specimen is under the in-plane compressive stress as a result of the difference of the thermal contraction between MnSi and CaF_2 (Fig. S2 of the Supplemental Material [38]). In fact, it is known that the skyrmion phase enlarges toward low temperatures when a compressive stress is applied perpendicular to a magnetic-field direction [43].

B. Hall resistivity under current

We then measured ρ_{yx} under a DC electric current bias j_{dc}, particularly, focusing on the resulting changes in the THE signal. The results are displayed as broken curves in Fig. 1(d). We found that under $j_{DC} = 7.7\times10^8$ A/m^2, the top-hat-shaped signal almost disappears, and, accordingly, ρ_{yx} varies smoothly with the magnetic field, whereas the other profiles remain nearly unchanged. This feature is also captured by a color map of $\Delta\rho_{yx} \equiv \rho_{yx}(j_{DC} = 7.7\times10^8\ \mathrm{A/m^2}) - \rho_{yx}(j_{DC} = 0)$ as shown in Fig. 1(e) where the red open circles delimit the region in which the THE signal is observed during the field-decreasing process when the DC current bias is off. These observations indicate that the application of a DC current bias exclusively affects the skyrmion phase. The detailed j_{dc} dependence further reveals that ρ_{yx} changes at $j_{DC} = 2.5\text{–}4\times10^8$ A/m^2, above which the ρ_{yx} value depends on j_{DC} only weakly [Fig. 1(f)]; hence, the absence of the THE is not a property that manifests only at a certain current density but rather can be viewed as a characteristic of the high-current regime.

In considering these current-induced phenomena, we will first show that the suppression of the THE is not due to a (hypothetical) Joule-heating-driven thermodynamic transition from the skyrmion phase to a topologically trivial magnetic phase at a higher temperature, such as a conical or ferromagnetic phase (below, we collectively refer to these phases as nonskyrmionic phases for simplicity). The following two experimental results should be highlighted. First, we did not observe a current-induced THE signal. If a Joule-heating-driven thermodynamic transition were present, the current-induced transition in the opposite direction (that is, from the nonskyrmionic conical phase to the skyrmion phase at a higher temperature) would also occur, which would be signified in blue in Fig. 1(e). This is clearly not the case in these experiments. Second, the sample-temperature increase estimated from the resistivity data is only ∼0.2–0.3 K (Fig. S3 of the Supplemental Material [38]), too small to explain the THE suppression observed over the wide temperature range of 19–24 K. Moreover, our finite-element simulation on the Joule heating reveals that even if the local temperature increase due to the Joule heating is considered, a current-heating-induced transition is still unlikely (for more details, see the Supplemental Material and Fig. S4 [38]). These experimental and numerical observations, thus, lead us to conclude that the Joule heating plays a minor role in the present experiment.

We, thus, consider a nonthermal mechanism for the suppression of the THE. As mentioned, two possibilities can be conceived as the nonequilibrium steady state that emerges from the original skyrmion phase by applying current: a steady skyrmion flow, as previously reported for bulk [31,32] and periodic-boundary systems [33,34], or a different magnetic state as a result of a current-induced phase change. To gain more insight into this issue, we measured the time evolution of the Hall resistivity $\rho_{yx}(t)$ [Fig. 2(a)]. Note that the experiments were performed for the thermal equilibrium skyrmion phase, which was prepared by a field cooling from a temperature higher than the magnetic ordering to a target temperature. As expected from the ρ_{yx}-H profile shown in Fig. 1(d), when $j_{DC} = 8.3\times10^8$ A/m^2 is applied (for clarity, the pulse width was intentionally set to be long, 100 s), $|\rho_{yx}|$ begins to be suppressed and reasonably settles to a value corresponding to no THE. We note that due to the measurement time constant and the abrupt switching of the electric circuit in the present experiment, the Hall resistivity was not measured correctly during the ∼ 30 s after the DC current was switched on or off (the data in the time duration are, therefore, shaded in gray. See also Fig. S5 in the Supplemental Material [38]). What is noteworthy here is that even after the current is switched off, the reduced $|\rho_{yx}|$ remains at a similar level, thus, excluding the scenario in which the suppression of the THE signal is due to a steady skyrmion flow, which should cease when the DC current supply is stopped. By contrast, this observation is reasonably accounted for by the alternative scenario in which the application of the current triggers a nonthermal phase change from the skyrmion phase into another magnetic phase, in the present case, in a nonvolatile manner.

The latter scenario can also be tested by checking whether a characteristic found in other nonequilibrium phase transitions is observed in this current-induced phenomenon. We note that numerical studies on various types of nonequilibrium phase transitions including photoinduced phase transitions often observe that a stronger excitation results in a shorter timescale to complete the transition [44–46]. In the present experiment, the low time resolution prevented real-time observation of the intrinsic phase-evolution dynamics during the current application; nevertheless, because of the nonvolatile nature of the current-induced phenomenon, we could still probe the time evolution of the suppression of the THE signal simply by measuring the postpulse ρ_{yx} value. We, thus, investigated the THE suppression while varying the pulse amplitude and width (Fig. 2(b), the raw data of which are shown in Fig. S6 of the Supplemental Material [38]) and found that the pulse width required to completely suppress the THE becomes shorter as the applied current density increases. This observation highlights the strong correlation between the driving force and the phase-evolution dynamics, confirming that the present current-induced phenomenon exhibits a characteristic of nonequilibrium phase transitions.

The experimental results demonstrate that the equilibrium skyrmion-lattice phase can be suppressed by applying current in a nonvolatile manner to the extent that the THE signal almost disappears. Previous studies on bulk MnSi [42,47] and CoFeB [48] multilayer systems have reported a current-induced global phase change from a thermodynamically stable nonskyrmionic state to a metastable skyrmion-condensed state (thus, the phase transition is in the opposite direction of the present result). These mechanisms rely on a thermal effect; that is, the Joule-heating-induced transition to a thermodynamically stable skyrmion phase at a higher temperature, followed by thermal quenching. By

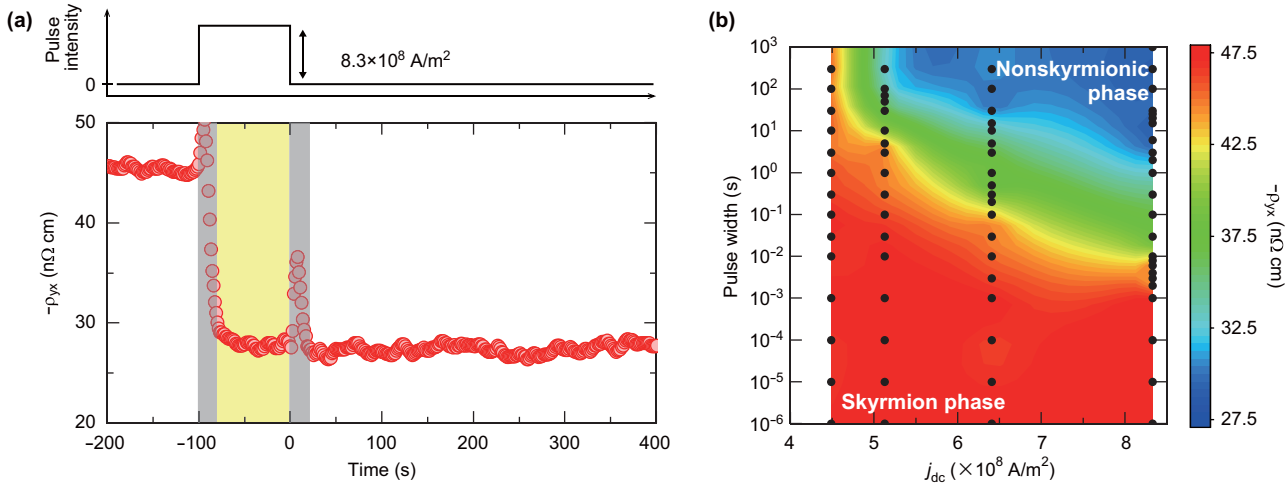

FIG. 2. Current-induced nonvolatile nonequilibrium topological transition from the skyrmion phase to a nonskyrmionic phase. (a) Time profile of ρ_{yx} under switching on/off of a DC current bias. The yellow-hatched region indicates the period of application of the DC current. During the ∼30 s after the DC current was switched on or off, ρ_{yx} was not measured correctly due to the measurement time constant. The measurement was performed at $T = 19.0$ K and $\mu_0 H = 0.22$ T. (b) Contour plot of nonequilibrium phase-change evolution as a function of the DC current bias and pulse width. The color represents the postpulse value of ρ_{yx}. The black dots represent the set of parameters at which the measurements were performed. The measurements were performed at $T = 20.4$ K and $\mu_0 H = 0.22$ T. The raw data are shown in Fig. S6 of the Supplemental Material [38].

contrast, the current-induced phase change addressed in this paper occurs through a nonthermal mechanism, and it should, therefore, be distinguished from Joule-heating-induced transitions triggered by current.

C. Metastability of the current-induced state

Let us now discuss the nature of the current-induced state in more detail. First, from the fact that the thermal equilibrium phase is the skyrmion phase, one can immediately see that the current-induced state is metastable in the absence of flowing current and, hence, should have a finite lifetime due to the recovery to the equilibrium skyrmion phase, which is the most likely final state of the relaxation. To characterize the nature of such a metastable state from the $\rho_{yx}(t)$ profile, it is convenient to consider a time-dependent volume fraction of the skyrmion phase by introducing a quantity $\phi(t) \equiv [\rho_{yx}(t) - \rho_{yx}^{DC}]/[\rho_{yx}^{before} - \rho_{yx}^{DC}]$, where ρ_{yx}^{before} and ρ_{yx}^{DC} are the equilibrium or steady-state values before and during the application of a DC current, respectively. With this quantity, we can compare the time profiles $\phi(t)$ at different temperatures as shown in Fig. 3(a) (the $\rho_{yx}(t)$ profiles are shown in Fig. S7 of the Supplemental Material [38]). A slow recovery from the current-induced state with no THE ($\phi = 0$) to the equilibrium skyrmion phase ($\phi = 1$) can be clearly seen especially at high temperatures, indicating that the current-induced state is not a true stable state in the absence of flowing current. The full recovery of the true equilibrium state, namely, the skyrmion phase, appears to require a length of time far beyond 10^4 s; furthermore, the initial relaxation process cannot be correctly measured due to the measurement time constant ∼ 30 s (Fig. S5 of the Supplemental Material [38]). Because of this limited time range over which relaxation phenomena were observed, it was difficult to derive a quantitative relaxation time by fitting to, for instance, an exponential function. To experimentally characterize the stability of the current-induced state at a qualitative level, we, therefore, used the value $1 - \phi(t)$ after a long elapsed time $t = 10^4$ s. The temperature dependence of this value demonstrates that the stability of the current-induced state degrades as the temperature increases [Fig. 3(b)], consistent with the general tendency that a metastable phase has a shorter lifetime at higher temperatures [42,49,50].

D. Magnetic structure of the current-induced state

The remaining issue of importance is the magnetic structure of the current-induced state. However, obtaining a clear answer to this question is difficult due to the lack of operando real-space observations. Nevertheless, important insights can be derived from the following two observations. First, because the emergent magnetic phase exhibits no THE, it is immediately clear that it is a nonskyrmionic phase. Second, the current-induced magnetic phase is metastable in the absence of flowing current, implying that it is a competing order with a free energy close to that of the skyrmion phase. According to the bulk phase diagram [Fig. 1(c)], the second-lowest free-energy phase after the thermodynamically stable skyrmion phase should be the conical phase, which is, thus, considered to be the most likely current-induced phase.

This insight gained from free-energy considerations can be further verified by checking whether the magnetic-field dependence of the stability of the current-induced state is consistent with that would be expected for the conical phase. In general, when considering the stability of a metastable state, the free-energy difference between the equilibrium and the metastable states is an important factor because it is the driving force for the system to reach the equilibrium state. The free-energy difference between the conical and the skyrmion phases is, thus, of interest, and we note that this quantity

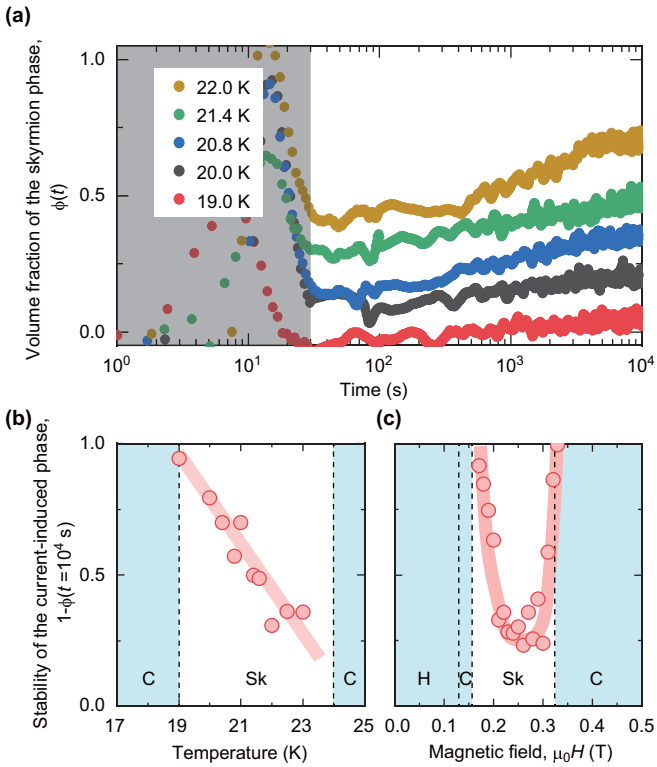

FIG. 3. Slow recovery of the equilibrium skyrmion phase and stability of the current-induced state. (a) Time evolution of the skyrmion-phase volume fraction after the DC electric current is switched off at different temperatures. A pulse with a duration of 100 s was used to ensure sufficient conversion of the equilibrium skyrmion phase into a nonskyrmionic phase. The time origin $t = 0$ represents the time when the current was switched off. The shaded area represents the time period during which the measured values are not correct due to the measurement time constant. The measurement was performed at $\mu_0 H = 0.22$ T. The time evolution of the corresponding ρ_{yx} value is displayed in Fig. S7 of the Supplemental Material [38]. (b) and (c) Isomagnetic-field temperature dependence (b) and isothermal magnetic-field dependence (c) of the stability of the current-induced phase. In (b) and (c), the various equilibrium phases, such as "C" (conical), "Sk" (skyrmion), and "H" (helical), are also represented by referring to Fig. 1(c). The measurements in (b) and (c) were performed at $\mu_0 H = 0.22$ T and $T = 22.5$ K, respectively.

vanishes on the phase boundary by definition (Fig. S8 of the Supplemental Material [38]). The magnetic-field dependence of $1 - \phi(t = 10^4\ \text{s})$, which is an indicator of the stability of the current-induced state, is plotted in Fig. 3(c). It can be seen that the stability is weakest at the center of the skyrmion phase and strongest at the upper- and lower-field phase boundaries between the skyrmion and the conical phases. Such nonmonotonic metastability is indeed consistent with what would be expected for the conical phase (for a more detailed explanation, see the Supplemental Material [38]), thereby supporting the scenario in which the current-induced phase is the conical phase. Conversely, if we assume that the current-induced state is a ferromagnetic or helical phase, it is difficult to explain the nonmonotonic stability profile, which is aligned with the skyrmion/conical phase boundaries.

E. Numerical simulations

Finally, let us discuss how ubiquitous such current-induced nonvolatile magnetic phase transitions are. For this purpose, it would be instructive to see whether such a phase transition can occur even in the simplest two-dimensional square-lattice spin model that exhibits a skyrmion phase (see Materials and Methods). Figure 4(a) shows the ground-state phase diagram of this model with respect to a magnetic-field h that is normal to the plane [33,51]. In this model, the skyrmion phase competes with the helical phase in the low-field regime and with the ferromagnetic phase in the high-field regime. Thus, it should be noted that the phase diagram of this numerical model is different from that of the microfabricated MnSi in which the skyrmion phase is surrounded by the conical phase [Fig. 1(c)]. If a similar current-induced nonvolatile phase transition is also observed in the minimal model, it means that the presence of this phenomenon does not depend on the details of the equilibrium magnetic phase diagram. It may, therefore, be useful to study the minimal model even if the phase diagram is different from that of the microfabricated MnSi. The behavior under a DC spin current j_s has been well studied within the framework of the standard Landau-Lifshitz-Gilbert equation and established for the corresponding model with periodic boundaries [29,32]; for instance, the skyrmion lattice state at equilibrium exhibits a steady flow at $j_s = 0.01$ while maintaining its lattice structure.

In contrast, we found that the model with open boundaries does not exhibit a steady skyrmion flow but instead undergoes a current-induced nonvolatile change from the skyrmion phase to a nonskyrmionic phase. Figures 4(b) and 4(c) display the time evolution under the same magnitude of $j_s (= 0.01)$ at $h = 0.02$ and 0.025, respectively. As time progresses, the skyrmions exit the system from the right boundary, whereas no new skyrmions are supplied from the left; as a result, the number of skyrmions remaining in the system decreases with time [Figs. 4(b) and 4(c)], and after a sufficiently long elapsed time, only a small number of skyrmions remain. Interestingly, the emergent magnetic order that replaces the initial skyrmion phase varies with h: It is helical for $h = 0.02$ [Fig. 4(b)] and ferromagnetic for $h = 0.025$ [Fig. 4(c)]. We also found that these emergent magnetic orders persist even after the current injection ceases; that is, the current-induced phase is nonvolatile.

The h-dependent current-induced magnetic order deserves further discussion. We consider this issue from an energy perspective as before and, thus, analyze the energy hierarchy of this model. The results shown in Fig. 4(d) demonstrate that the phase competing with the skyrmion phase is helical in the low-field regime ($h \leqslant 0.025$) and ferromagnetic in the high-field regime ($h > 0.025$). Intriguingly, this overall tendency is in line with the h-dependent current-induced magnetic order [Figs. 4(b) and 4(c)]. We note that this agreement holds only at a qualitative level, such as whether the current-induced phase is a helical-like spin-winding state or a ferromagnetic-like spin-polarized state; to be precise, the current-induced phase is neither ideally helical nor ideally ferromagnetic as found at equilibrium. Nevertheless, this qualitative agreement suggests that there exists an intimate correlation between the emergent magnetic state under a current and the energy

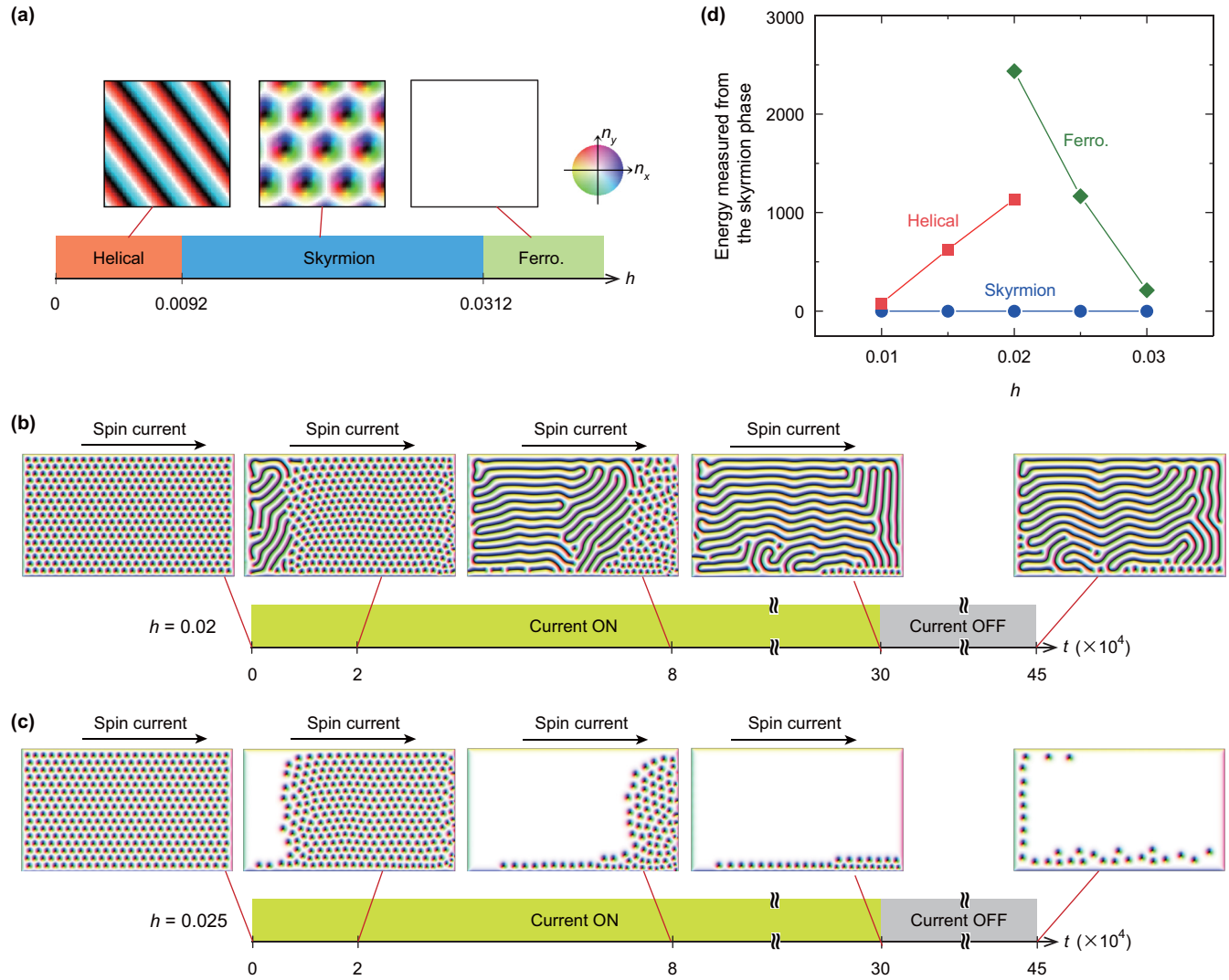

FIG. 4. Micromagnetic simulations of current-induced magnetic phase transitions in an open-boundary system. (a) Ground-state magnetic phase diagram of the Hamiltonian [Eq. (1)] with respect to the magnetic-field h [33,50]. The color wheel specifies the magnetization direction on the x-y plane. The brightness of the color represents the z component of the magnetization; that is, local magnetizations pointing fully in the z direction are displayed as white. (b) and (c) Snapshots of the evolution of the current-induced magnetic phase change at $h = 0.02$ (b) and 0.025 (c). The magnitude of the DC spin-polarized current j_s is 0.01. The unit of time is $1/(\gamma J)$ (see Materials and Methods). (d) Magnetic-field-dependent energy hierarchies of the helical skyrmion and ferromagnetic phases in the Hamiltonian [Eq. (1)].

hierarchy at equilibrium. We also note that this energy perspective is the same as the approach that we used to understand the magnetic-field-dependent stability of the current-induced phase observed in the microfabricated MnSi.

III. CONCLUDING REMARKS

We have found current-induced nonvolatile magnetic transitions from the skyrmion phase to nonskyrmion phases in two different skyrmion systems: Experimentally in microfabricated MnSi and through simulations in a two-dimensional system with open boundaries; remarkably, the current-induced transitions are not fractional but involves a global change in magnetism, comparable to that accompanies the corresponding thermodynamic phase transition of the whole system. The magnetic phase diagrams of the two systems are different, and this fact, in turn, implies that current-induced global phase transitions are inherent to various skyrmion-hosting systems. As mentioned above, it is known that a steady skyrmion flow is realized under a DC current in a bulk crystal of MnSi [31,32] and in simulations of a two-dimensional system with periodic boundaries [29,33,34]. Given this fact, it is safe to say that the current-induced magnetic phase transitions reported here are a characteristic of spatially confined small-sized systems in which both the system boundaries and the bulk are expected to play important roles; on the other hand, the critical sample dimension, below which the skyrmion steady flow is inhibited and instead the current-induced phase transition occurs, remains to be clarified. From a broader perspective, the present observations imply that even if small-sized and bulk materials exhibit similar physical properties at equilibrium, each system can exhibit qualitatively different nonequilibrium phases of matter. Perhaps a tantalizing variety of novel nonequilibrium phenomena and their applications in

quantum materials should be explored with attention to the system size.

ACKNOWLEDGMENTS

F.K. thanks S. Yonezawa, H. Ito, and T. Oka for valuable discussions. This work was partially supported by JSPS KAKENHI (Grants No. 20H01866, No. 20K03810, No. 21H04442, No. 18H05225, and No. 18H03676) and JST CREST (Grants No. JPMJCR20T1 and No. JPMJCR1874).

APPENDIX: MATERIALS AND METHODS

1. Sample preparations

A MnSi single crystal was grown via the Czochralski method. The sample was fabricated using a FIB into a microsized (approximately) bar-shaped specimen ($18.0\times1.3\times1.2\ \mu\mathrm{m}^3$) with axes along the three equivalent [100] directions [Figs. 1(a) and 1(b)]. For the details of the sample geometry, see Fig. S1 in the Supplemental Material [38].

2. Transport measurements

The Hall resistivity ρ_{yx} was measured at 33 Hz with an AC current excitation ($\approx 7.7\times10^7\ \mathrm{A/m^2}$) under a magnetic field parallel to the $\langle 100\rangle$ axis using lock-in amplifiers (Stanford Research Systems SR830) with a lock-in time constant of 3 s and a 24 dB/oct roll-off, equipped with a preamplifier (NF Corporation SA410-F3). The DC+AC electric currents were generated by a function generator (NF Corporation WF1947) with/without a DC electric current bias j_{DC} along the x direction. Hence, the Hall resistivity under a DC electric current is defined as $\rho_{yx}(j_{\mathrm{DC}}) \equiv dE_y/dj_{\mathrm{DC}}|_{j_{\mathrm{DC}}}$. The transport properties are reproducible, thereby, indicating that applying a current of up to $8.3\times10^8\ \mathrm{A/m^2}$ does not cause any detectable damage to the specimen.

3. Micromagnetic simulation

Simulations were performed for a simple square lattice consisting of 1000×580 magnetic moments with open boundary conditions in the x and y directions. We considered the following model Hamiltonian,

$$\mathcal{H} = -J\sum_{\boldsymbol{r}} \boldsymbol{n}_{\boldsymbol{r}}\cdot(\boldsymbol{n}_{\boldsymbol{r}+\hat{\boldsymbol{x}}}+\boldsymbol{n}_{\boldsymbol{r}+\hat{\boldsymbol{y}}}) \tag{A1}$$

$$+ D\sum_{\boldsymbol{r}}(\boldsymbol{n}_{\boldsymbol{r}}\times\boldsymbol{n}_{\boldsymbol{r}+\hat{\boldsymbol{x}}}\cdot\hat{\boldsymbol{x}}+\boldsymbol{n}_{\boldsymbol{r}}\times\boldsymbol{n}_{\boldsymbol{r}+\hat{\boldsymbol{y}}}\cdot\hat{\boldsymbol{y}}) \tag{A2}$$

$$- h\sum_{\boldsymbol{r}} n_{z,\boldsymbol{r}}, \tag{A3}$$

where J is the exchange interaction, D is the Dzyaloshinskii-Moriya interaction energy, h is the magnetic field along the z direction, $\hat{\boldsymbol{x}}$ (or $\hat{\boldsymbol{y}}$) is the unit vector of the connection to the nearest neighbor site along the x (or y) direction, $\boldsymbol{n}_{\boldsymbol{r}}$ is the unit vector of the local magnetic moment at site $\boldsymbol{r}$, and $n_{z,\boldsymbol{r}}$ is the z component of $\boldsymbol{n}_{\boldsymbol{r}}$. When simulating the current-induced dynamics of the skyrmions at zero temperature, we inserted the Hamiltonian into the following Landau-Lifshitz-Gilbert equation,

$$\frac{d\boldsymbol{n}_{\boldsymbol{r}}}{dt} = -\gamma\frac{d\mathcal{H}}{d\boldsymbol{n}_{\boldsymbol{r}}}\times\boldsymbol{n}_{\boldsymbol{r}} + \alpha\boldsymbol{n}_{\boldsymbol{r}}\times\frac{d\boldsymbol{n}_{\boldsymbol{r}}}{dt} - (\boldsymbol{v}_s\cdot\nabla)\boldsymbol{n}_{\boldsymbol{r}} + \beta[\boldsymbol{n}_{\boldsymbol{r}}\times(\boldsymbol{v}_s\cdot\nabla)\boldsymbol{n}_{\boldsymbol{r}}], \tag{A4}$$

where $\boldsymbol{v}_s = v_s\hat{\boldsymbol{x}}$ represents the spin current density, which is related to the electric current density through $\boldsymbol{v}_s = -(pd^3/2e)\boldsymbol{j}$. The effect of the so-called nonlocal damping [52] was not taken into account because the previous results to be compared also did not consider this effect. The units of dimensionless time t, velocity v, and electric current j are $1/(\gamma J)$ ($\approx 6.5\times10^{13}$ s), $d\gamma J$ ($\approx 7.7\times10^2$ m/s), and $2e\gamma J/pd^2$ ($\approx 1.0\times10^{13}\ \mathrm{A/m^2}$), respectively, where e (>0) is the elementary charge, γ is the gyromagnetic ratio, p is the polarization of the magnet, and d is the lattice constant of the square lattice. We chose the following parameter set: $\{J = 1.0, D = 0.2, \alpha = \beta = 0.04$, and $j = 0.01\}$.

[1] A. Asamitsu, Y. Tomioka, H. Kuwahara, and Y. Tokura, Current switching of resistive states in magnetoresistive manganites, Nature **388**, 50 (1997).

[2] R. Kumai, Y. Okimoto, and Y. Tokura, Current-induced insulator-metal transition and pattern formation in an organic charge-transfer complex, Science **284**, 1645 (1999).

[3] F. Nakamura, M. Sakaki, Y. Yamanaka, S. Tamaru, T. Suzuki, and Y. Maeno, Electric-field-induced metal maintained by current of the Mott insulator Ca_2RuO_4, Sci. Rep. **3**, 2536 (2013).

[4] I. Valmianski, P. Y. Wang, S. Wang, J. G. Ramirez, S. Guénon, and I. K. Schuller, Origin of the current-driven breakdown in vanadium oxides: Thermal versus electronic, Phys. Rev. B **98**, 195144 (2018).

[5] R. Waser and M. Aono, Nanoionics-based resistive switching memories, Nat. Mater. **6**, 833 (2007).

[6] A. Sawa, Resistive switching in transition metal oxides, Mater. Today **11**, 28 (2008).

[7] V. Guiot, L. Cario, E. Janod, B. Corraze, V. T. Phuoc, M. Rozenberg, P. Stoliar, T. Cren, and D. Roditchev, Avalanche breakdown in $GaTa_4Se_{8-x}Te_x$ narrow-gap Mott insulators, Nat. Commun. **4**, 1722 (2013).

[8] J. Zhang, A. S. McLeod, Q. Han, X. Chen, H. A. Bechtel, Z. Yao, S. N. Gilbert Corder, T. Ciavatti, T. H. Tao, M. Aronson, G. L. Carr, M. C. Martin, C. Sow, S. Yonezawa, F. Nakamura, I. Terasaki, D. N. Basov, A. J. Millis, Y. Maeno, and M. Liu, Nano-Resolved Current-Induced Insulator-Metal Transition in the Mott Insulator Ca_2RuO_4, Phys. Rev. X **9**, 011032 (2019).

[9] Y. Kalcheim, A. Camjayi, J. D. Valle, P. Salev, M. Rozenberg, and I. K. Schuller, Non-thermal resistive switching in Mott insulator nanowires. Nat. Commun. **11**, 2985 (2020).

[10] M. Yamanouchi, D. Chiba, F. Matsukura, and H. Ohno, Current-induced domain-wall switching in a ferromagnetic semiconductor structure, Nature **428**, 539 (2004).

[11] S. S. P. Parkin, M. Hayashi, and L. Thomas, Magnetic domain-wall racetrack memory, Science **320**, 190 (2008).
[12] S. Emori, U. Bauer, S.-M. Ahn, E. Martinez, and G. S. D. Beach, Current-driven dynamics of chiral ferromagnetic domain walls, Nat. Mater. **12**, 611 (2013).
[13] E. B. Myers, D. C. Ralph, J. A. Katine, R. N. Louie, and R. A. Buhrman, Current-induced switching of domains in magnetic multilayer devices, Science **285**, 867 (1999).
[14] J. A. Katine, F. J. Albert, R. A. Buhrman, E. B. Myers, and D. C. Ralph, Current-Driven Magnetization Reversal and Spin-Wave Excitations in Co/Cu/Co Pillars, Phys. Rev. Lett. **84**, 3149 (2000).
[15] J. Grollier, P. Boulenc, V. Cros, A. Hamzić, A. Vaurès, and A. Fert, Switching a spin valve back and forth by current-induced domain wall motion, Appl. Phys. Lett. **83**, 509 (2003).
[16] M. Tsoi, A. G. M. Jansen, J. Bass, W.-C. Chiang, M. Seck, V. Tsoi, and P. Wyder, Excitation of a Magnetic Multilayer by an Electric Current, Phys. Rev. Lett. **80**, 4281 (1998).
[17] S. I. Kiselev, J. C. Sankey, I. N. Krivorotov, N. C. Emley, R. J. Schoelkopf, R. A. Buhrman, and D. C. Ralph, Microwave oscillations of a nanomagnet drinven by a spin-polarized current, Nature **425**, 380 (2003).
[18] V. E. Demidov, S. Urazhdin, and S. O. Demokritov, Direct observation and mapping of spin waves emitted by spin-torque nano-oscillators, Nat. Mater. **9**, 984 (2010).
[19] S. Maekawa, S. O. Valenzuela, E. Saitoh, and T. Kimura, *Spin Current*, 2nd ed. (Oxford University Press, Oxford, 2017).
[20] K. Dolui, M. D. Petrović, K. Zollner, P. Plecháč, J. Fabian, and B. K. Nikolić, Proximity spin-orbit torque on a two-dimensional magnet within van der waals heterostructure: Current-driven antiferromagnet-to-ferromagnet reversible nonequilibrium phase transition in bilayer CrI_3, Nano Lett. **20**, 2288 (2020).
[21] A. Bogdanov and D. A. Yablonskii, Thermodynamically stable "vortices" in magnetically ordered crystals. The mixed state of magnets, Zh. Eksp. Teor. Fiz. **95**, 178 (1989) [Sov. Phys. JETP **68**, 101 (1989)].
[22] A. Bogdanov and A. Hubert, Thermodynamically stable magnetic vortex states in magnetic crystals, J. Magn. Magn. Mater. **138**, 255 (1994).
[23] S. Mühlbauer, B. Binz, F. Jonietz, C. Pfleiderer, A. Rosch, A. Neubauer, R. Georgii, and P. Böni, Skyrmion lattice in a chiral magnet, Science **323**, 915 (2009).
[24] X. Z. Yu, Y. Onose, N. Kanazawa, J. H. Park, J. H. Han, Y. Matsui, N. Nagaosa, and Y. Tokura, Real-space observation of a two-dimensional skyrmion crystal, Nature **465**, 901 (2010).
[25] N. Nagaosa and Y. Tokura, Topological properties and dynamics of magnetic skyrmions, Nat. Nanotechnol. **8**, 899 (2013).
[26] A. Fert, V. Cros, and J. Sampaio, Skyrmions on the track, Nat. Nanotechnol. **8**, 152 (2013).
[27] J. Sampaio, V. Cros, S. Rohart, A. Thiaville, and A. Fert, Nucleation, stability and current-induced motion of isolated magnetic skyrmions in nanostructures, Nat. Nanotechnol. **8**, 839 (2013).
[28] J. Iwasaki, M. Mochizuki, and N. Nagaosa, Current-induced skyrmion dynamics in constricted geometries, Nat. Nanotechnol. **8**, 742 (2013).
[29] S.-Z. Lin, C. Reichhardt, C. D. Batista, and A. Saxena, Driven Skyrmions and Dynamical Transitions in Chiral Magnets, Phys. Rev. Lett. **110**, 207202 (2013).
[30] S. Woo, K. Litzius, B. Krüger, M.-Y. Im, L. Caretta, K. Richter, M. Mann, A. Krone, R. M. Reeve, M. Weigand, P. Agrawal, I. Lemesh, M.-A. Mawass, P. Fischer, M. Kläui, and G. S. D. Beach, Observation of room-temperature magnetic skyrmions and their current-driven dynamics in ultrathin metallic ferromagnets, Nat. Mater. **15**, 501 (2016).
[31] F. Jonietz, S. Mühlbauer, C. Pfleiderer, A. Neubauer, W. Münzer, A. Bauer, T. Adams, R. Georgii, P. Böni, R. A. Duine, K. Everschor, M. Garst, and A. Rosch, Spin transfer torques in MnSi at ultralow current densities, Science **330**, 1648 (2010).
[32] T. Schulz, R. Ritz, A. Bauer, M. Halder, M. Wagner, C. Franz, C. Pfleiderer, K. Everschor, M. Garst, and A. Rosch, Emergent electrodynamics of skyrmions in a chiral magnet, Nat. Phys. **8**, 301 (2012).
[33] J. Iwasaki, M. Mochizuki, and N. Nagaosa, Universal current-velocity relation of skyrmion motion in chiral magnets, Nat. Commun. **4**, 1463 (2013).
[34] C. Reichhardt, D. Ray, and C. J. O. Reichhardt, Collective Transport Properties of Driven Skyrmions with Random Disorder, Phys. Rev. Lett. **114**, 217202 (2015).
[35] A. W. Teixeira, S. Castillo-Sepulveda, L. G. Rizzi, A. S. Nunez, R. E. Troncoso, D. Altbir, J. M. Fonseca, and V. L. Carvalho-Santos, Motion-induced inertial effects and topological phase transitions in skyrmion transport, J. Phys.: Condens. Matter **33**, 265403 (2021).
[36] A. Neubauer, C. Pfleiderer, B. Binz, A. Rosch, R. Ritz, P. G. Niklowitz, and P. Böni, Topological Hall Effect in the A Phase of MnSi, Phys. Rev. Lett. **102**, 186602 (2009).
[37] A. Bauer and C. Pfleiderer, Magnetic phase diagram of MnSi inferred from magnetization and ac susceptibility, Phys. Rev. B **85**, 214418 (2012).
[38] See Supplemental Material at http://link.aps.org/supplemental/10.1103/PhysRevB.106.144425 for extended experimental data, supporting data analysis, and discussions, which includes Refs. [53–58].
[39] M. Lee, Y. Onose, Y. Tokura, and N. P. Ong, Hidden constant in the anomalous Hall effect of high-purity magnet MnSi, Phys. Rev. B **75**, 172403 (2007).
[40] J. Ye, Y. B. Kim, A. J. Millis, B. I. Shraiman, P. Majumdar, and Z. Tešanović, Berry Phase Theory of the Anomalous Hall Effect: Application to Colossal Magnetoresistance Manganites, Phys. Rev. Lett. **83**, 3737 (1999).
[41] P. Bruno, V. K. Dugaev, and M. Taillefumier, Topological Hall Effect and Berry Phase in Magnetic Nanostructures, Phys. Rev. Lett. **93**, 096806 (2004).
[42] H. Oike, A. Kikkawa, N. Kanazawa, Y. Taguchi, M. Kawasaki, Y. Tokura, and F. Kagawa, Interplay between topological and thermodynamic stability in a metastable magnetic skyrmion lattice, Nat. Phys. **12**, 62 (2016).
[43] Y. Nii, T. Nakajima, A. Kikkawa, Y. Yamasaki, K. Ohishi, J. Suzuki, Y. Taguchi, T. Arima, Y. Tokura, and Y. Iwasa, Uniaxial stress control of skyrmion phase Nat. Commun. **6**, 8539 (2015).
[44] A. Ono and S. Ishihara, Double-Exchange Interaction in Optically Induced Nonequilibrium State: A Conversion from Ferromagnetic to Antiferromagnetic Structure, Phys. Rev. Lett. **119**, 207202 (2017).
[45] Y. Murakami, N. Tsuji, M. Eckstein, and P. Werner, Nonequilibrium steady states and transient dynamics of conventional

superconductors under phonon driving, Phys. Rev. B **96**, 045125 (2017).

[46] F. Peronaci, S. Ameli, S. Takayoshi, A. Landsman, and T. Oka, Mott memristors based on field-induced carrier avalanche multiplication, arXiv:2104.00559.

[47] T. Nakajima, H. Oike, A. Kikkawa, E. P. Gilbert, N. Booth, K. Kakurai, Y. Taguchi, Y. Tokura, F. Kagawa, and T. Arima, Skyrmion lattice structural transition in MnSi, Sci. Adv. **3**, e1602562 (2017).

[48] I. Lemesh, K. Litzius, M. Böttcher, P. Bassirian, N. Kerber, D. Heinze, J. Zázvorka, F. Büttner, L. Caretta, M. Mann, M. Weigand, S. Finizio, J. Raabe, M.-Y. Im, H. Stoll, G. Schütz, B. Dupé, M. Kläui, and G. S. D. Beach, Current-induced skyrmion generation through morphological thermal transitions in chiral ferromagnetic heterostructures, Adv. Mater. **30**, 1805461 (2018).

[49] D. R. Uhlmann, A kinetic treatment of glass formation, J. Non-Cryst. Solids **7**, 337 (1972).

[50] I. Vaskivskyi, J. Gospodaric, S. Brazovskii, D. Svetin, P. Sutar, E. Goreshnik, I. A. Mihailovic, T. Mertelj, and D. Mihailovic, Controlling the metal-to-insulator relaxation of the metastable hidden quantum state in 1T-TaS_2, Sci. Adv. **1**, e1500168 (2015).

[51] M. Mochizuki, Spin-Wave Modes and Their Intense Excitation Effects in Skyrmion Crystals, Phys. Rev. Lett. **108**, 017601 (2012).

[52] S. Zhang and S. S.-L. Zhang, Generalization of the Landau-Lifshitz-Gilbert Equation for Conducting Ferromagnets, Phys. Rev. Lett. **102**, 086601 (2009).

[53] S. M. Stishov, A. E. Petrova, S. Khasanov, G. Kh. Panova, A. A. Shikov, J. C. Lashley, D. Wu, and T. A. Lograsso, Experimental study of the magnetic phase transition in the MnSi itinerant helimagnet, J. Exp. Theor. Phys. **106**, 888 (2008).

[54] A. C. Bailey and B. Yates, The low-temperature thermal expansion and vibrational properties of alkaline earth fluorides, Proc. Phys. Soc., London **91**, 390 (1967).

[55] S. M. Stishov, A. E. Petrova, S. Khasanov, G. Kh Panova, A. A. Shikov, J. C. Lashley, D. Wu, and T. A. Lograsso, Heat capacity and thermal expansion of the itinerant helimagnet MnSi, J. Phys.: Condens. Matter **20**, 235222 (2008).

[56] H.-M. Eiter, P. Jaschke, R. Hackl, A. Bauer, M. Gangl, and C. Pfleiderer, Raman study of the temperature and magnetic-field dependence of the electronic and lattice properties of MnSi, Phys. Rev. B **90**, 024411 (2014).

[57] G. A. Slack, Thermal conductivity of CaF_2, MnF_2, CoF_2, and ZnF_2 crystals, Phys. Rev. **122**, 1451 (1961).

[58] H. Oike, M. Kamitani, Y. Tokura, and F. Kagawa, Kinetic approach to superconductivity hidden behind a competing order, Sci. Adv. **4**, eaau3489 (2018).